

Inositol Phosphate Recycling Regulates Glycolytic and Lipid Metabolism That Drives Cancer Aggressiveness

Daniel I. Benjamin,[†] Sharon M. Louie,[†] Melinda M. Mulvihill,[†] Rebecca A. Kohnz,[†] Daniel S. Li,[†] Lauryn G. Chan,[†] Antonio Sorrentino,[§] Sourav Bandyopadhyay,^{||} Alyssa Cozzo,[†] Anayo Ohiri,[†] Andrei Goga,^{‡,§,||} Shu-Wing Ng,[⊥] and Daniel K. Nomura*,[†]

[†]Program in Metabolic Biology, Department of Nutritional Sciences and Toxicology, University of California, Berkeley, Berkeley, California 94720, United States

[‡]Department of Cell and Tissue Biology, [§] Division of Hematology/Oncology, and ^{||}San Francisco Helen Diller Family Comprehensive Cancer Center, University of California, San Francisco, San Francisco, California 94143, United States

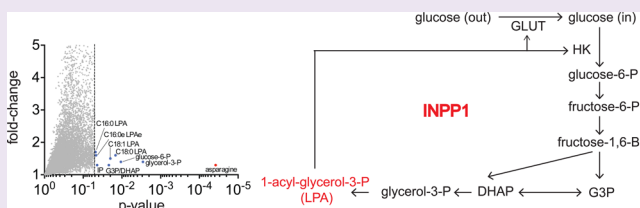
[⊥]Laboratory of Gynecologic Oncology, Brigham and Women's Hospital, Harvard Medical School, Boston, Massachusetts 02115, United States

S Supporting Information

ABSTRACT: Cancer cells possess fundamentally altered metabolism that supports their pathogenic features, which includes a heightened reliance on aerobic glycolysis to provide precursors for synthesis of biomass. We show here that inositol polyphosphate phosphatase 1 (INPP1) is highly expressed in aggressive human cancer cells and primary high-grade human tumors. Inactivation of INPP1 leads to a reduction in glycolytic intermediates that feed into the synthesis of the oncogenic signaling lipid lysophosphatidic acid (LPA), which in turn impairs LPA signaling and further attenuates glycolytic metabolism in a feed-forward mechanism to impair cancer cell motility, invasiveness, and tumorigenicity. Taken together these findings reveal a novel mode of glycolytic control in cancer cells that can serve to promote key oncogenic lipid signaling pathways that drive cancer pathogenicity.

Cancer cells undergo a fundamental reprogramming of key biochemical pathways that fuel cell proliferation. These alterations include an addiction to aerobic glycolysis (known as the Warburg effect), heightened lipogenesis, as well as an increase in glutamine-dependent anaplerosis.^{1,2} However, the metabolic reprogramming that drives the aggressive features of cancer, such as motility, invasiveness, and tumor-initiating capacity, is not well-understood. Since most cancer deaths are related to aggressive features of cancer, understanding the metabolic pathways that contribute to these pathogenic features of cancer is critical for both diagnosis and treatment.

We previously identified a gene expression signature of commonly dysregulated metabolic enzymes that were heightened across a panel of highly aggressive human cancer cells, leading us to hypothesize that there was a metabolic program that supports cancer malignancy.³ Consistent with this premise, two of these enzymes, monoacylglycerol lipase (MAGL) and KIAA1363, have been previously shown to be important in maintaining aggressive and tumorigenic features of cancer through modulating protumorigenic fatty acid or ether lipid derived signaling molecules, respectively.^{3–6} Here, we show that inositol polyphosphate phosphatase 1 (INPP1), another enzyme found in this gene expression signature, is highly upregulated across aggressive human cancer cells and high-grade primary human tumors. The established biochemical role



of INPP1 is to dephosphorylate free polyphosphorylated inositols.⁷ While INPP1 has been previously shown to be upregulated in human colorectal cancers, the role of this enzyme in cancer has remained obscure.⁸ In this study, we show that INPP1 drives cancer pathogenicity through controlling glycolytic pathways that feed into the generation of oncogenic signaling lipids. We find that inactivation of INPP1 impairs aggressive and tumorigenic features of cancer through impairing protumorigenic lipid signals derived from glycolytic metabolism.

RESULTS AND DISCUSSION

INPP1 Activity Is Upregulated in Aggressive Cancer Cells and Primary Human Tumors. Gene expression analysis comparing a panel of aggressive breast, prostate, ovarian, and melanoma cancer cell lines with their less aggressive counterparts⁴ previously revealed a commonly dysregulated signature of metabolic enzymes. These aggressive cancer cells do not show heightened proliferative capacity (Supplementary Figure S1A) but exhibit high migratory, invasive, and tumor-forming capacity compared to the less

Received: November 1, 2013

Accepted: April 16, 2014

Published: April 16, 2014



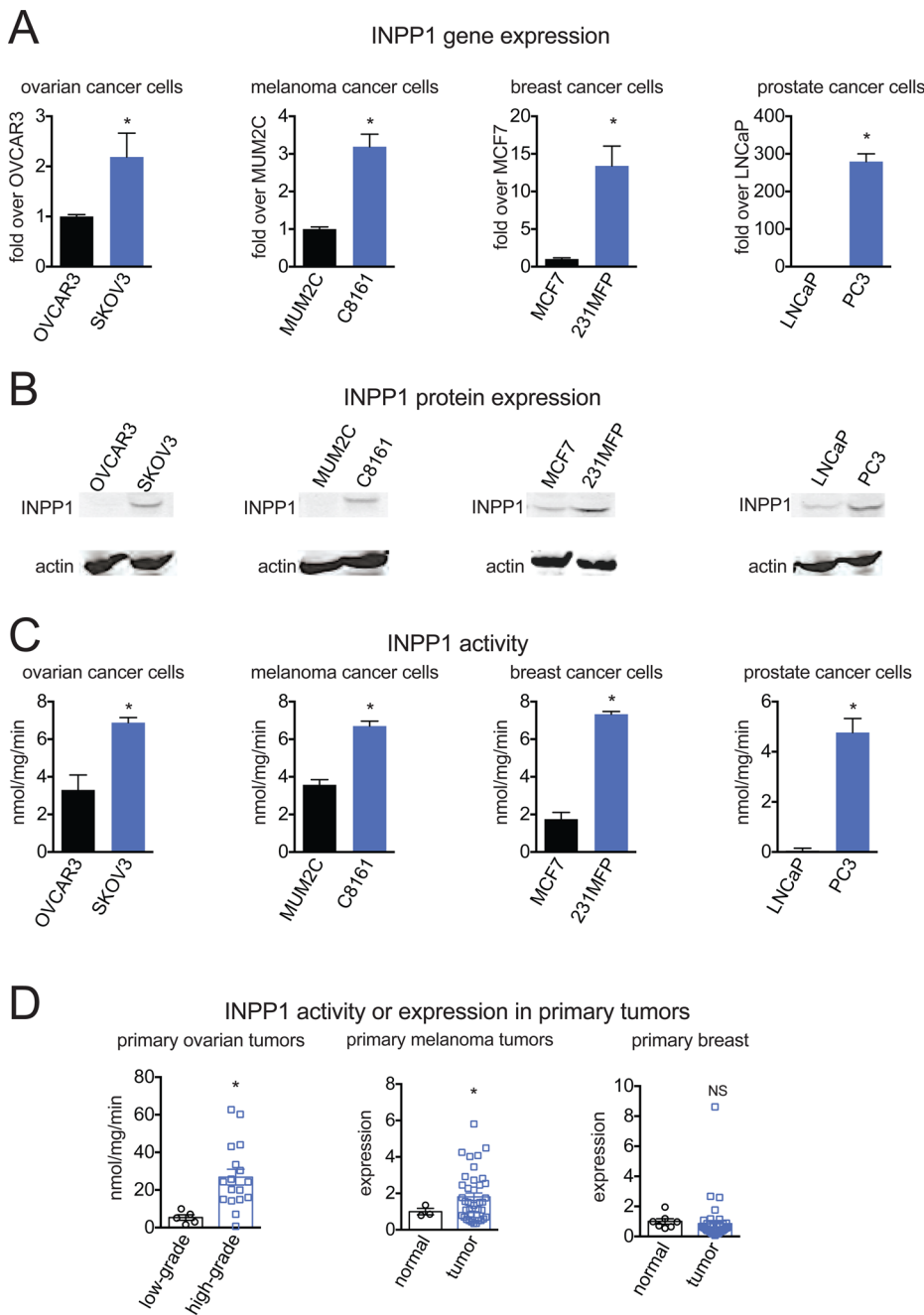


Figure 1. INPP1 is highly expressed in aggressive cancer cells and primary tumors. (A–C) INPP1 gene (A) and protein (B) expression and INPP1 activity (C) across aggressive ovarian, melanoma, breast, and prostate cancer cells (SKOV3, C8161, 231MFP, and PC3) compared to their less aggressive counterparts (OVCAR3, MUM2C, MCF7, and LNCaP) as measured by quantitative PCR (qPCR) (A), Western blotting (B), and inositol-1,4-bisphosphate phosphatase activity measuring inositol phosphate product formation by LC–MS (C). (D) INPP1 enzyme activity (for ovarian tumors) and mRNA expression (for melanoma and breast tumors) in high-grade compared to low-grade primary human ovarian tumors or melanoma or breast tumors compared to normal tissue. * $p < 0.05$. Data are presented as mean \pm SEM; $n = 3\text{--}5/\text{group}$ for panels A–C and $n = 3\text{--}39$ for panel D.

aggressive cancer cells.³ Among this signature, hydroxypruvate isomerase (HYI) and INPP1 were the only enzymes that act upon small-molecule substrates, exhibit a greater than 2-fold higher expression across aggressive cancer cells, and have also not been previously studied in cancer. INPP1 inactivation with RNA interference, but not HYI knockdown, led to migratory defects in cancer cells (Supplementary Figure S1B). Thus, we decided to focus our subsequent efforts on investigating the role of INPP1 in cancer. We find that INPP1 expression, protein levels, and enzyme activity are significantly elevated

across aggressive melanoma, prostate, ovarian, and breast cancer cells compared to their less aggressive counterparts (Figure 1A–C). INPP1 activity or expression is also significantly elevated in high-grade primary ovarian and melanoma tumors compared to low-grade ovarian tumors and normal skin tissue, respectively (Figure 1D). INPP1 was not differentially expressed in primary human breast tumors (Figure 1D). INPP1 protein expression is also upregulated upon overexpression of several commonly mutated or amplified human oncogenes (PI3KCA, activated MAP kinase

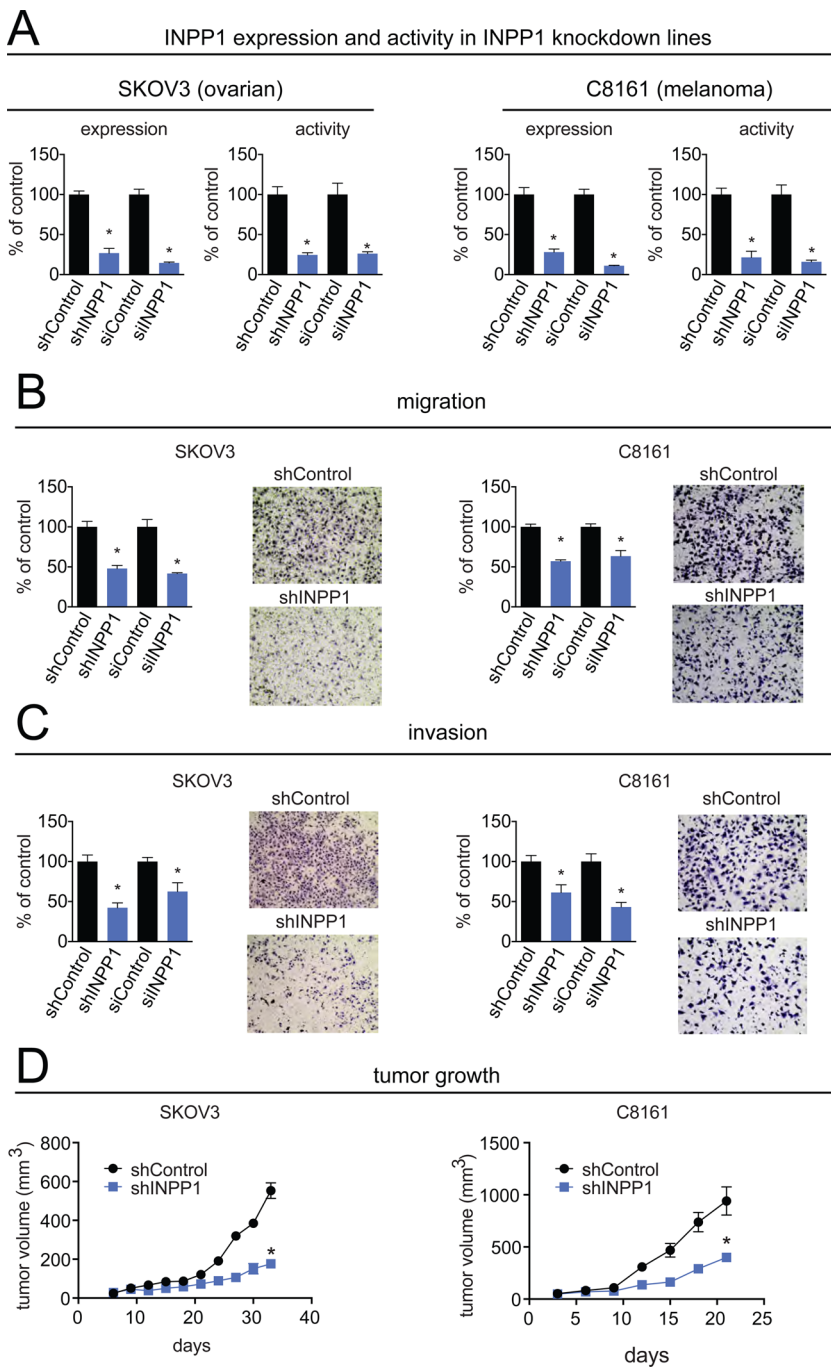


Figure 2. INPP1 inactivation leads to impairments in cancer pathogenicity. (A) INPP1 was knocked down using both a short-hairpin RNA (shRNA) oligonucleotide (shINPP1) as well as small-interfering RNA (siRNA) oligonucleotide (siINPP1), resulting in >70% reduction in both INPP1 expression and activity in C8161 and SKOV3 cells compared to their respective sh and siControl cells. (B,C) shINPP1 and siINPP1 cells show decreased migration (B) and invasion (C) compared to shControl and siControl cells in both SKOV3 and C8161 cells. Migration and invasion assays were performed by transferring cancer cells to serum-free media for 4 h prior to seeding 50,000 cells into inserts with 8 μ m pore size containing membranes coated with collagen (10 μ g/mL) or BioCoat Matrigel, respectively. C8161 and SKOV3 migration times were 5 and 8 h, respectively. Migrated or invaded cells refer to average numbers \pm SEM per four fields counted at 400 X magnification. (D) shINPP1 cells show impaired tumor growth in SCID mice compared to shControl cells. A total of 2×10^6 C8161 or SKOV3 cells/100 μ L were injected subcutaneously into the flank, and tumor growth was measured using calipers. Significance is presented as * p < 0.05 compared to shControl or siControl. Data are presented as mean \pm SEM; n = 3 or 4/group for panels A–C and n = 5 or 6/group for panel D.

(MEKDD1), HRAS, NeuNT, and BRAF) in MCF10A nontransformed mammary epithelial cells (Supplementary Figure S1C). These oncogenes have been previously associated with both transformation of cancer cells and acquisition of cancer malignancy.^{9–11} Taken together, our results indicate that INPP1 expression is heightened in aggressive cancer cells and

primary human ovarian and melanoma tumors and upon induction of MCF10A cells by several human oncogenes.

Disruption of INPP1 Impairs Cancer Pathogenicity. We next sought to ascertain the pathophysiological role of INPP1 in cancer. Since INPP1 is upregulated in high-grade human ovarian and melanoma tumors, but not in primary

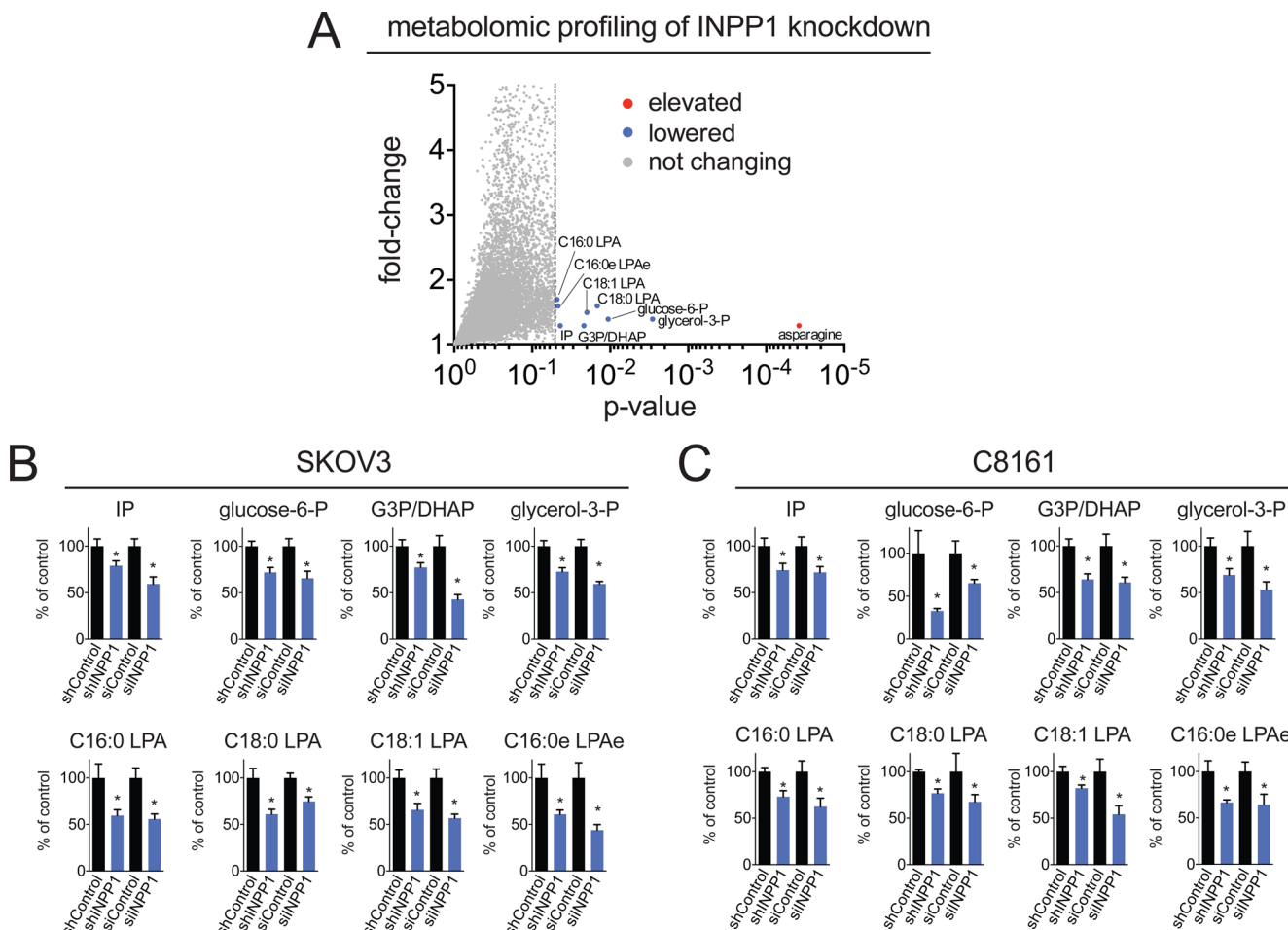


Figure 3. Metabolomic profiling links INPP1 to glycolysis and lipid metabolism. (A) Metabolomic analyses of cancer cell steady-state metabolomes with impaired INPP1 activity compared to control cells. The volcano plot shows all ions that were detected by targeted or untargeted metabolomic profiling of shControl and shINPP1 SKOV3 cells. Gray points show the ions and metabolites that were not significantly altered between shControl and shINPP1 cells. The red and blue points to the right of the dotted black line are metabolites that were significantly ($p < 0.05$) and commonly elevated or lowered, respectively, across C8161 and SKOV3 sh and siINPP1 compared to their respective sh and siControl cells. C16:0, C18:0, C18:1 refer to acyl chain length:unsaturation on LPA. C16:0e LPAe refers to the ether lipid counterpart of LPA (LPA-ether). All targeted data are in Supplementary Table S1. (B,C) Levels of metabolites that were altered upon INPP1 knockdown in SKOV3 (B) and C8161 (C) cells, quantified by SRM. Data are presented as means \pm SEM of $n = 4$ or 5/group with significance expressed as * $p < 0.05$ for INPP1 knockdown compared to control.

human breast tumors, we focused our attention on the role of INPP1 in ovarian and melanoma cancer cells. We knocked down the expression of INPP1 in both aggressive and less aggressive SKOV3 and OVCAR3 ovarian and C8161 and MUM2C melanoma cancer cells with short-hairpin (shINPP1) or small-interfering (siINPP1) RNA oligonucleotides, respectively, resulting in a 70–80% reduction in INPP1 expression, protein level, and activity (Figure 2A; Supplementary Figure S1D,E). INPP1 inactivation significantly impairs cancer cell migration and invasiveness in both the aggressive and less aggressive ovarian and melanoma cancer cells, without effects on cellular proliferation or serum-free cell survival (Figure 2B,C; Supplementary Figure S1E–G). We confirmed the specificity of the INPP1 knockdown effects by recapitulating our antimigratory effects with two independent siRNA oligonucleotides for INPP1 as well as partially to fully rescuing the migratory defect with reinforced expression of INPP1 in siINPP1 SKOV3 cells (Supplementary Figure S1E,H). Since INPP1 was discovered as upregulated across aggressive cancer cells that possess heightened migratory, invasive, and tumorigenic properties but are not more proliferative, we

interpret our results to indicate that INPP1 may be more important in maintaining aggressive or tumor-initiating features of cancer. Consistent with this premise, INPP1 inactivation in SKOV3 and C8161 cells slows tumor xenograft growth in immune-deficient mice (Figure 2D). These data indicate that INPP1 is necessary to maintain cancer cell motility, invasiveness, and tumorigenicity in ovarian and melanoma cancer cells both *in situ* and *in vivo*.

We overexpressed INPP1 in the ovarian cancer cells OVCAR3 and SKOV3 and melanoma cancer cells MUM2C but did not observe increases in cell migration, invasiveness, proliferation, or survival, indicating that INPP1 alone may not be sufficient to confer malignant properties to cancer cells (data not shown).

INPP1 Controls the Levels of Glycolytic Intermediates and Oncogenic Signaling Lipids. While INPP1 is known for its role in inositol phosphate metabolism, we were perplexed by how this role could affect cancer pathogenicity. We thus performed a large-scale metabolomic profiling study to identify metabolites that may be altered upon inactivation or overexpression of INPP1 in cancer cells, using single reaction

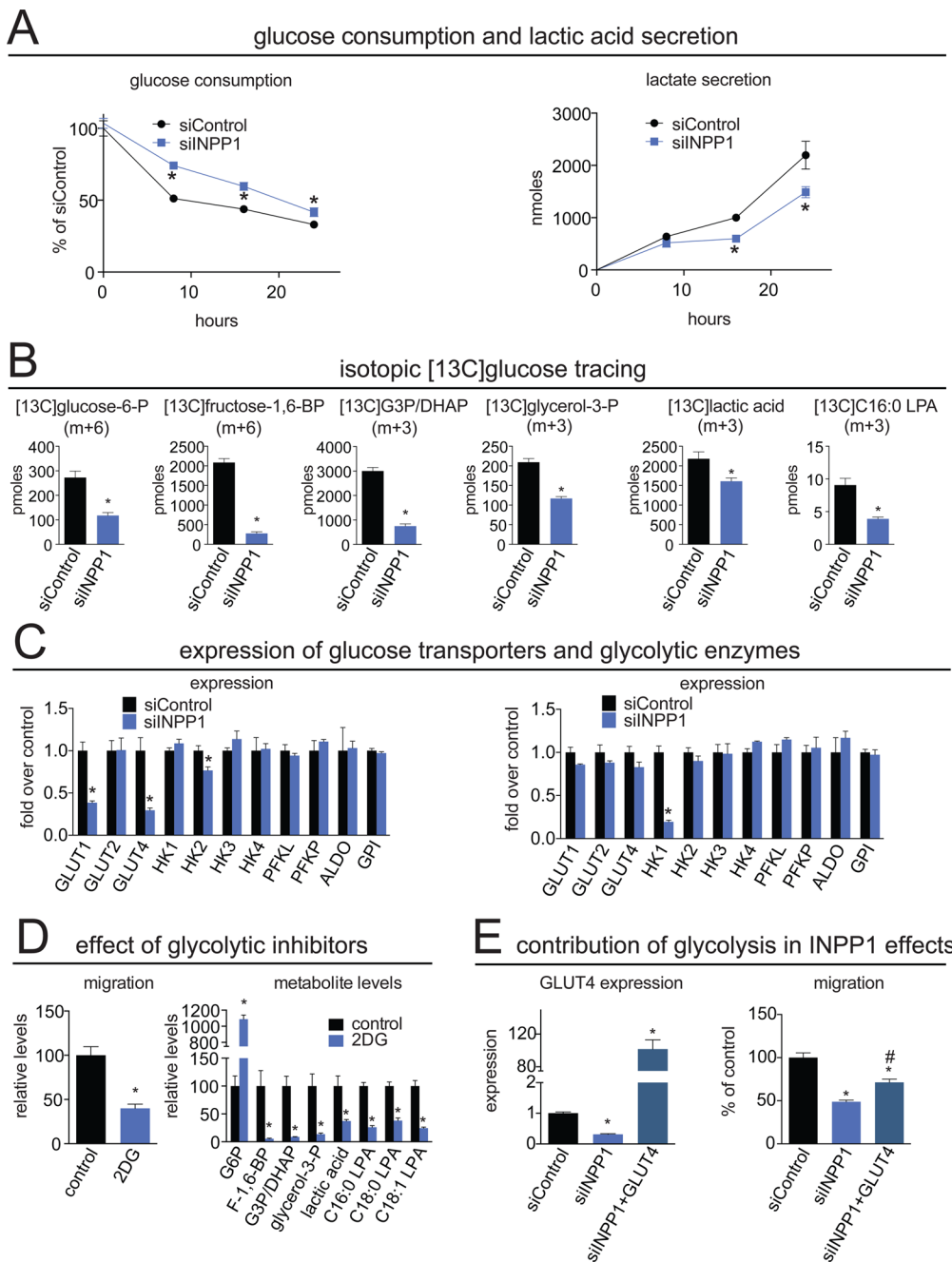


Figure 4. INPP1 modulates glycolytic and glucose-derived LPA metabolism. (A) Media glucose and lactate levels at 0, 8, 16, and 24 h in siControl and siINPP1 cells, measured by glucose assay kit and SRM-based LC–MS/MS, respectively. (B) Steady-state isotopic [¹³C] incorporation into glycolytic intermediates from treatment of siControl and siINPP1 SKOV3 cells with either 10 mM concentration of nonisotopic glucose or 10 mM concentration of isotopic [^{U-¹³C}]glucose for 24 h in otherwise glucose-free RPMI1640 media. Confirmation that we are measuring isotopic glycolytic intermediates at steady state is provided in Supplementary Figure S4. Full isotopomer distribution of metabolites is shown in Supplementary Figure S5. (C) Relative gene expression by qPCR of glucose transporters and glycolytic enzymes in SKOV3 and C8161 cells of siControl (black) compared with siINPP1 (blue) cells. (D) Phenotypic and metabolic effects of 2-deoxyglucose (2-DG) in SKOV3 cells. Treatment of SKOV3 cells with 2-DG (in water, 5 mM, 24 h) impairs SKOV3 cell migration (right panel) and lowers post-PGI glycolytic intermediates and LPA levels (left panel). (E) GLUT4 overexpression partially rescues migratory deficits conferred by INPP1 knockdown in SKOV3 cells. qPCR of GLUT4 expression is shown in the left panel, and migration data are shown in the right panel. Data are presented as means \pm SEM of $n = 3\text{--}5$ /group with significance expressed as * $p < 0.05$ compared to siControl or control cells and # $p < 0.05$ comparing siINPP1+GLUT4 to siINPP1 groups.

monitoring (SRM)-based targeted methods as well as untargeted liquid chromatography–mass spectrometry (LC–MS)-based metabolomic platforms. We quantitatively measured >130 metabolites using SRM-based targeted methods and $>12,000$ ions with our untargeted methods coupled to bioinformatic analysis using XCMSOnline¹² (Figure 3A–C)

(targeted data shown in Supplementary Table S1). Upon filtering for metabolites that were commonly and significantly altered in both sh and siINPP1 cells in both SKOV3 and C8161 lines, we find that INPP1 inactivation leads to reductions in the levels of the product of INPP1, inositol phosphate (IP), as well as reductions in glycolytic intermediates glucose-6-phosphate

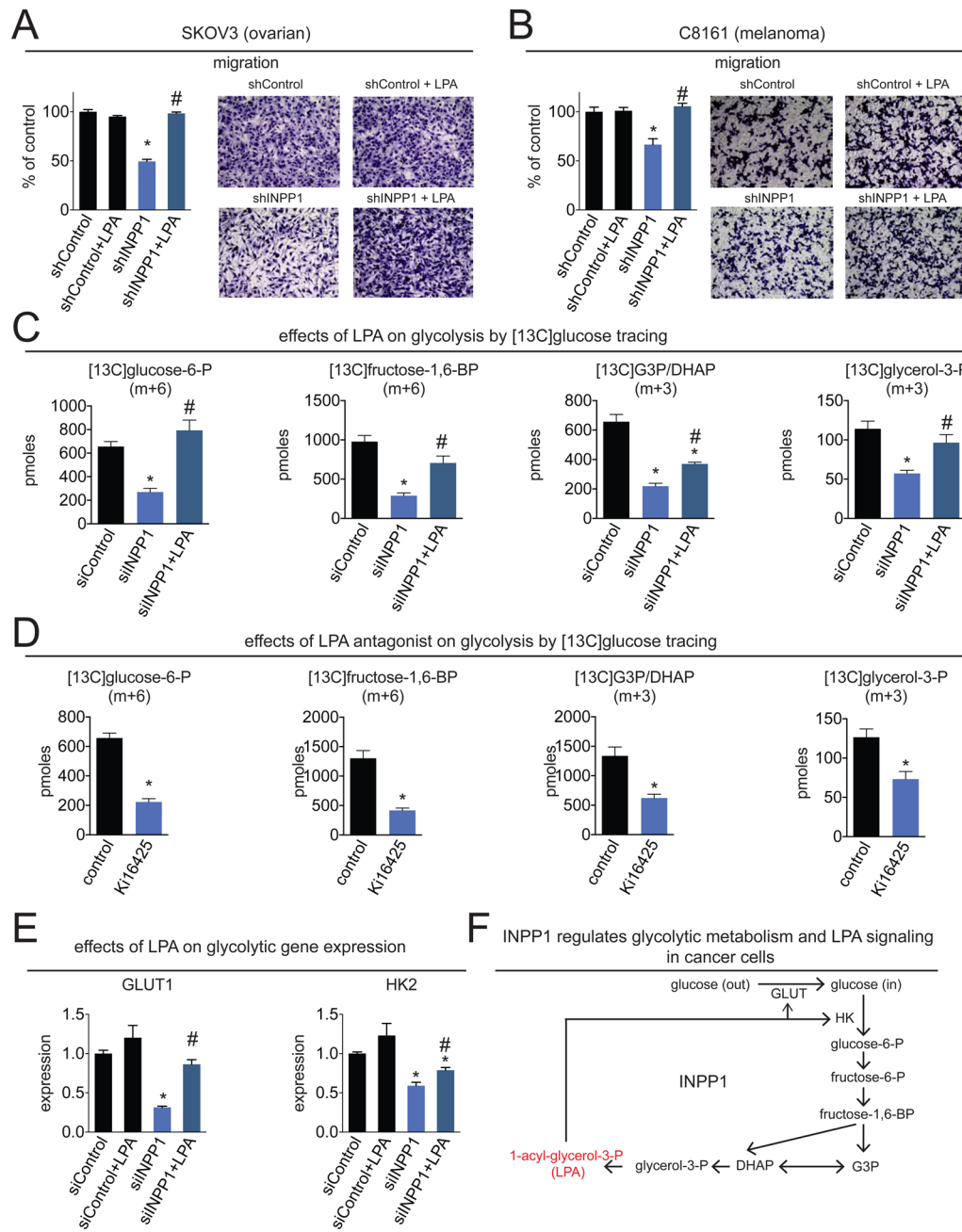


Figure 5. LPA modulates the migratory defects and glycolytic impairments conferred by INPP1 knockdown. (A,B) The migratory impairment in siINPP1 SKOV3 ovarian (A) and C8161 melanoma (B) cells is fully rescued upon treating cells with low concentrations of LPA (100 nM). Treatment with DMSO or LPA (100 nM) was initiated concurrently with the seeding of cells for assessment of cancer cell migration (24 h). (C) Reduced [¹³C] incorporation into glycolytic intermediates from labeling siINPP1 cells with [¹³C]glucose (24 h) is rescued upon treatment of cells with LPA (1 μM). Treatment with LPA was initiated 2 days after transfection of siINPP1 oligonucleotides and 24 h prior to labeling of cells with either [¹²C] or [¹³C]glucose (10 mM, 24 h). (D) Isotopic incorporation into glycolytic intermediates is reduced upon treating SKOV3 cells with the LPA antagonist Ki16425 (10 μM). The antagonist or DMSO was pretreated with SKOV3 cells 24 h prior to seeding of cells for labeling with [¹²C] or [¹³C]glucose (10 mM, 24 h). For panels C and D, isotopic incorporation of [¹³C]glucose into glycolytic intermediates and glycerol-3-phosphate were quantified by SRM-based LC–MS/MS. (E) The reduction in GLUT1 and HK2 expression conferred by INPP1 knockdown is partially to fully rescued by LPA (1 μM). (F) Model depicting the metabolic role of INPP1 in controlling glycolytic metabolism and LPA signaling. Data are average ± SEM, $n = 3\text{--}5/\text{group}$. Significance is expressed in panels A, B, and E as * $p < 0.05$ comparing shControl to all other groups and # $p < 0.05$ comparing the LPA-treated shINPP1 to DMSO-treated shINPP1 groups. Significance in panel C is expressed as * $p < 0.05$ comparing siINPP1 with siControl groups and # $p < 0.05$ comparing LPA-treated siINPP1 with DMSO-treated siINPP1 groups. Significance in panel D is expressed as * $p < 0.05$ comparing Ki16425-treated and DMSO-treated groups.

(glucose-6-P) and glyceraldehyde-3-phosphate/dihydroxyacetone phosphate (G3P/DHAP), metabolites in glycerophospholipid synthesis glycerol-3-phosphate (glycerol-3P) and lysophosphatidic acid (LPA) levels, and the ether lipid LPA-

ether (LPAe) (Figure 3A–C; Supplementary Table S1). We also observe increases in the levels of the amino acid asparagine. Additional changes in other glycolytic intermediates were also observed in siINPP1 SKOV3 and C8161 cells, including as

fructose-6-phosphate (fructose-6-P) and fructose-1,6-bisphosphate (fructose-1,6-BP) that are not observed in shINPP1 cells. This may be due to better knockdown of INPP1 with the si oligonucleotide compared with our shINPP1 lines (Supplementary Table S1 and Supplementary Figure S2A,B). The specificity of these metabolite changes were confirmed by two independent siRNA oligonucleotides targeting INPP1 as well as partial to full rescue of metabolite changes by reinforced expression of INPP1 in siINPP1 SKOV3 cells (Supplementary Figure S2A,B). While we could not detect important phosphatidylinositol species such as phosphatidylinositol bisphosphate due to limitations in our metabolomic profiling, other inositol polyphosphates, such as IP5 and IP6, were unchanged (Supplementary Figure S2C). Nonetheless, measuring phosphorylated phosphatidylinositol species will be of future interest and important in fully understanding the role of INPP1 in cancer.

While we do not yet understand how INPP1 alters asparagine levels, our results collectively indicate that INPP1 may modulate glycolytic pathways that feed into glycerophospholipid biosynthesis. Although INPP1 overexpression is not sufficient to confer increased aggressiveness in SKOV3 cells, it is sufficient to increase the levels of glycolytic intermediates and LPA (Supplementary Figure S3A,B). Taken together these results indicate that INPP1 is both necessary and sufficient to control the levels of glycolytic intermediates and LPA in cancer cells.

INPP1 Exerts Control over Glycolytic Metabolism and Glucose-Derived LPA Synthesis in Cancer Cells. Based on our metabolomic profiling data, we hypothesized that INPP1 inactivation was leading to impairments in glycolytic metabolism. Consistent with this premise, we find that INPP1 ablation decreases both media glucose consumption and lactate secretion in a time-dependent manner (Figure 4A). We also show that glucose consumption is significantly increased upon INPP1 overexpression in SKOV3 cells (Supplementary Figure S3C). Reinforcing this data, we also show that isotopic incorporation of [$U-^{13}C$]glucose into [^{13}C]glycolytic intermediates, glycerol-3-P, and LPA (^{13}C incorporation in the glycerol backbone) are also significantly lowered upon INPP1 knockdown under steady-state labeling conditions (Figure 4B, Supplementary Figure S4; full isotopomer analysis shown in Supplementary Figure S5). Taken together, these results indicate that INPP1 knockdown impairs glycolytic metabolism and glucose-derived LPA levels.

Given that glycolytic metabolism appears to be markedly impaired with INPP1 knockdown, we next asked whether the enzymes that are responsible for importing, trapping, or metabolizing glucose within the cell might be altered as well. Indeed, we find that INPP1 knockdown in SKOV3 cells leads to a marked downregulation in glucose transporter 1 (GLUT1), GLUT4, and hexokinase (HK2) expression, and we show partial to full reversal of these changes upon reinforced expression of INPP1 (Figure 4C, Supplementary Figure S6). Interestingly, we find that in C8161 cells, INPP1 knockdown leads to a downregulation in HK1 expression, but not GLUT1/4 or HK2 expression (Figure 4C). Taken together, our results indicate that INPP1 ablation may lead to impairments in glycolytic metabolism and lowering of glucose-derived LPA levels that are the result of transcriptional alterations to both glucose transporters and hexokinase.

On the basis of these metabolic alterations, we surmised that the pathogenic impairments conferred by INPP1 knockdown

might also result from lowered glycolysis and LPA synthesis. Indeed, we find that inhibition of glycolysis by the phosphoglucose isomerase (PGI) inhibitor 2-deoxyglucose (2DG) recapitulates the antimigratory phenotype and lowering of post-PGI glycolytic intermediates and LPA levels (Figure 4D). Furthermore, we show that the migratory impairments caused by INPP1 knockdown are partially rescued by enforced expression of GLUT4 (Figure 4E).

Regulation of Glycolytic Metabolism and Cancer Cell Pathogenicity by LPA. Next, we wanted to understand the mechanism through which INPP1 was modulating cancer pathogenicity and glycolytic and lipid metabolism. While our data suggested that we were impairing glycolytic metabolism, we discounted energetic impairments as a cause for the observed pathogenic impairments since ATP levels were not consistently lower in INPP1 knockdown SKOV3 and C8161 cells (Supplementary Table S1). Interestingly, LPA has been well-studied as a potent oncogenic signaling lipid that acts through LPA receptor signaling to drive multiple stages of cancer including migration, invasion, and tumorigenicity.¹³ We therefore hypothesized that INPP1 may be modulating cancer cell migration through controlling LPA synthesis and signaling. Consistent with this premise, low concentrations of LPA (100 nM), which did not stimulate basal migration, fully rescue the migratory defects conferred by INPP1 knockdown (Figure 5A,B), indicating that LPA may possibly be involved in the mechanism through which INPP1 drives cancer pathogenicity.

We next wanted to determine whether this reduced LPA signaling in INPP1 knockdown cells was also leading to decreased glycolytic metabolism. Consistent with this premise, we find that LPA rescues the impaired glycolytic metabolism that feeds into glycerol-3-P synthesis in siINPP1 SKOV3 cells (Figure 5C). We also find that LPA receptor antagonism (with Ki16425, 10 μ M¹⁴) reduces isotopic incorporation of [^{13}C]glucose into glycolytic intermediates and glycerol-3-P (Figure 5D). The transcriptional downregulation of GLUT1 and HK2 observed with INPP1 knockdown are also partially to fully rescued upon addition of LPA (Figure 5E). Thus, our results, though correlative, indicate that reduced LPA levels and LPA receptor signaling may in part be responsible for the glycolytic impairments observed upon INPP1 knockdown, which in turn may further lower glucose-derived LPA levels.

Since the PI3K/AKT and MAPK pathways have been shown to act downstream of LPA to exert control over both glucose transporters and glycolytic enzymes,^{1,15} we next asked whether the AKT or MAPK signaling pathway might be perturbed upon INPP1 inactivation under serum-free conditions. Paradoxically, we find that the levels of both phospho-AKT (p-AKT) and p-ERK are increased upon INPP1 knockdown (Supplementary Figures S7A,B). While we cannot fully explain these findings, Zhong et al. previously showed that inhibition of glycolysis by 2-DG also paradoxically leads to significant increases in both p-AKT and p-ERK, as a compensatory mechanism for maintaining cell survival.¹⁶ It may thus be possible that INPP1 knockdown and subsequent glycolytic impairments may upregulate AKT and MAPK signaling pathways to maintain cellular survival.

Recently, Yu et al. and Cai et al. discovered that LPA also acts upstream of the Hippo signaling pathway to promote the migration of ovarian cancer cells through the inhibition of the YAP kinase, LATS, resulting in the dephosphorylation and nuclear localization of YAP, activating a transcriptional program to promote cell migration.^{17,18} Interestingly, Cai et al. also

showed that LPA-induced YAP activation promotes the activation of downstream epidermal growth factor receptor (EGFR) signaling, which has previously been shown to drive glycolytic metabolism in cancer cells.^{18–20} Thus, the metabolic and pathophysiological effects observed with INPP1 inactivation may act through the Hippo transducer YAP. Indeed, we find that INPP1 knockdown significantly increases YAP phosphorylation (p-YAP), and this is partially rescued by addition of LPA (100 nM) (Figure 6A). We show that knockdown of YAP also impairs glucose consumption and lactic acid secretion, suggesting that YAP may influence glycolytic metabolism (Figure 6B).

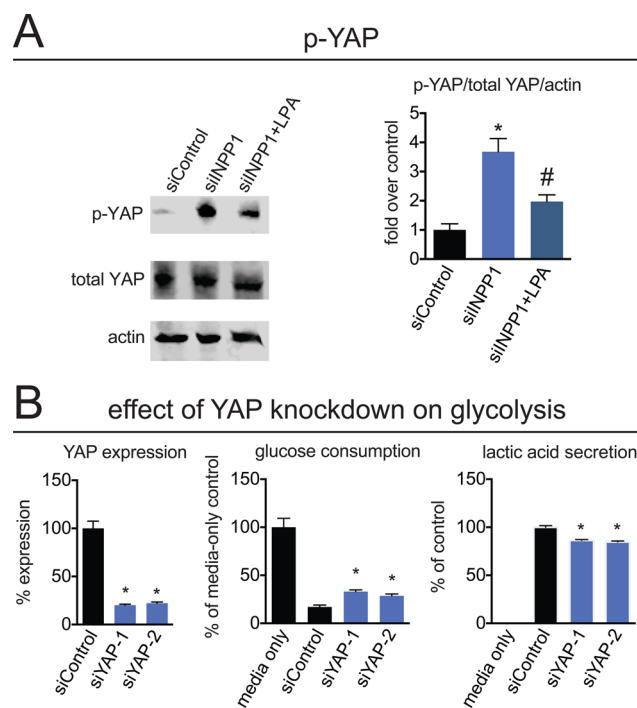


Figure 6. INPP1 knockdown affects the Hippo transducer YAP. (A) INPP1 knockdown increases phosphorylated YAP (p-YAP) protein levels compared to siControl cells in SKOV3 cells grown in serum-free media for 24 h by Western blotting. This increase in p-YAP is partially rescued upon addition of LPA (100 nM, 24 h). (B) YAP was knocked down by >75% in SKOV3 cells using two independent si oligonucleotides, and YAP knockdown was confirmed by qPCR. After 48 h of transfection with siControl or siYAP oligonucleotides, media was replaced, and media glucose and lactic acid levels were measured after 24 h by glucose assay kit and SRM-based LC–MS/MS, respectively. Data are represented as $n = 3\text{--}5/\text{group}$. Significance expressed as * $p < 0.05$ compared to siControl, # $p < 0.05$ comparing siINPP1+LPA to siINPP1.

Thus, we show that INPP1 inactivation leads to glycolytic impairments and lowering of glucose-derived LPA levels and that INPP1 ablation impairs cellular migration, invasiveness, and tumor growth in ovarian and melanoma cancer cells. While our results are still highly correlative and there are likely to be additional mechanisms mediating INPP1 effects upon cancer, we provide compelling evidence that INPP1 inactivation may impair cancer pathogenicity and glycolytic metabolism, through lowering LPA and possibly attenuating LPA-Hippo signaling pathways through heightened YAP phosphorylation.

Conclusion. In this study, we demonstrate INPP1 as a highly expressed metabolic enzyme in aggressive ovarian and

melanoma cancer cells and primary human tumors. We show that INPP1 is a unique metabolic node that controls glycolytic metabolism and glucose-derived LPA synthesis. We also show that INPP1 inactivation leads to impairments in cancer cell pathogenicity possibly through impaired LPA signaling through modulating the Hippo pathway.

A key critical question that remains is the mechanism of how INPP1 lowers LPA levels and signaling and how INPP1 affects glycolytic metabolism. It is still unclear whether lower LPA levels or impaired glycolytic metabolism occurs first upon INPP1 knockdown, but we provide compelling evidence that LPA and glycolytic metabolism are intricately linked and that INPP1 modulates this coupled metabolic and signaling programming in cancer cells. We surmise that a decrease in the downstream products (inositol phosphates and free inositol) or an increase in the upstream reactants (inositol polyphosphates) may lead to transcriptional changes within the cell that result in glycolytic impairment and/or a decrease in cellular LPA levels. Alternatively, there may be yet unknown inositol phosphate pathways that feed into supplying glycolytic intermediates or LPA that are initially lowered to instigate this process.

We previously showed that one of the enzymes upregulated across aggressive cancer cells, monoacylglycerol lipase (MAGL), was the primary lipolytic enzyme that released free fatty acids in cancer cells, which were remodeled into oncogenic signaling lipids such as LPA, prostaglandins, and other lysophospholipids.⁴ Quite interestingly, while MAGL provides the fatty acids to be esterified onto glycerophospholipids, INPP1, by controlling the cellular uptake of glucose, provides the glycerol-3-P backbone for this reaction, both collectively leading to the synthesis of LPA. We previously showed that MAGL conferred aggressive features to cancer cells also through modulating fatty acid-derived LPA and prostaglandin signaling. It will therefore be intriguing to determine whether blocking both INPP1 and MAGL leads to additive or synergistic effects by blocking both the generation of fatty acids and the glycerol-3-phosphate backbone for LPA synthesis.

In summary, we put forth INPP1 as a critical metabolic node that uniquely regulates glycolytic metabolism and oncogenic lipid signaling pathways to promote cancer motility, invasiveness, and tumorigenicity. Furthermore, we show that INPP1 mediates this effect on glycolysis possibly through LPA signaling, highlighting a unique intersection between lipid signaling pathways and central carbon metabolism in cancer cells. INPP1 may thus be an attractive therapeutic target for combatting malignant human cancers.

METHODS

Materials. All cell lines, with the exception of C8161, MUM2C, and 231MFP, were purchased from ATCC. The C8161 and MUM2C lines were provided by Mary Hendrix. The 231MFP cells were generated from explanted xenograft tumors of MDA-MB-231 cells, as described previously.²¹

Cell Culture Conditions. HEK293T cells were cultured in DMEM media containing 10% FBS and maintained at 37 °C with 5% CO₂. SKOV3 and C8161 cells were cultured in RPMI1640 media containing 10% FBS and glutamine maintained at 37 °C at 5% CO₂. PC3 cells were cultured in F12K media containing 10% FBS and glutamine and were maintained at 37 °C at 5% CO₂. 231MFP cells were cultured in L15 media containing 10% FBS and glutamine and were maintained at 37 °C in 0% CO₂.

Quantitative PCR. Quantitative PCR was performed using the manufacturer's protocol for Fischer Maxima SYBRgreen, with 10 μ M primer concentrations. Further methods are found in Supporting Information.

INPP1 Activity Assay. INPP1 phosphatase activity was measured by an adaptation of the assay described previously.⁷ Briefly, cell or tumor lysate (20 μ g protein) was incubated with the INPP1 substrate inositol-1,4-bisphosphate (50 μ M) for 60 min at RT in phosphate buffered saline with 50 μ M magnesium chloride (50 μ L total reaction volume). Heat denatured proteomes were used as a negative control. The reactions were quenched by the addition of 1:1 acetonitrile/methanol (200 μ L), followed by centrifugation (1300 rpm, 5 min) and collection of the supernatant for subsequent SRM-based LC–MS analysis quantitating the formation of inositol-4-phosphate product and subtracting background levels measured in heat-denatured proteome negative controls.

Human Primary Ovarian Tumors. Patients were diagnosed and treated for ovarian tumors at Brigham and Women's Hospital and Dana-Farber Cancer Center (Boston, MA, USA). All patient-derived biologic specimens were collected and archived under protocols approved by the Human Subjects Committee of the Brigham and Women's Hospital. The histopathologic diagnosis was determined by the gynecological pathologists at Brigham and Women's Hospital. The tumors were classified and graded according to the International Federation of Gynecology and Obstetrics (FIGO) system. For this work, 8 benign and 14 high-grade malignant ovarian tumor samples were used for the INPP1 activity and metabolite measurements. The benign cases included benign cysts, ovarian fibromas, and benign serous cystadenomas, whereas the malignant cases were all high-grade papillary serous carcinomas. Fresh tumor tissues were cut with scalpels into 2–5 mm pieces, individually wrapped in aluminum foil, snap-frozen in liquid nitrogen, and kept at –80 °C. INPP1 activity was measured as described above.

MCF10A Cell Line Generation and Screening. Derivative isogenic MCF10A cell lines were generated through stable infection using viral infection of cell pools using either pLX304, pMSCV-Hygro, or pMSCV-puro vectors. Control MCF10A cell lines were generated by expressing empty vectors conferring puromycin or blasticidin gene resistance as appropriate. Overexpression of genes was confirmed by Western blotting with specific antibodies.

Constructing INPP1 Knockdown Cells. We used both short-hairpin (sh) and small-interfering (si) RNA using two independent silencing oligonucleotides to knockdown the expression of INPP1. For construction of stable shRNA knockdown lines, lentiviral plasmids (pLKO.1) containing shRNA (purchased from Open Biosystems) against human INPP1 were transfected into HEK293 cells using Fugene (Roche). Lentivirus was collected from filtered culture media (0.45 μ m filters) and delivered to the target cancer cell line with Polybrene. These target cells were subsequently selected over 3 days with 1 μ g/mL puromycin. For transient knockdown of INPP1 with siRNA (Dharmacon), cells were seeded in 6-cm dishes (200,000 cells) for 24 h and then transfected with siRNA per manufacturer's instructions. The short-hairpin sequence used for constructing shINPP1 was as follows: CCGGGCTTAGAAAGAAATCCAGAA-ACTCGAGTTCTGGATTTCTTCTAACTGTTTG. The control shRNA was targeted against green fluorescent protein with the target sequence GCAAGCTGACCTGAAGTTCAT. The pooled small-interfering RNAs used to generate the siINPP1 lines were as follows: CUGCAGAGACGCAUACCUA, GCAAAGGUCCUCA-AUGGUAA, GGUAGCAUCUGAAGCAUUA, CCAAUGAGUUUA-CUAAUGA. The individual siRNAs 1–4 for INPP1 used in Supplementary Figure S1 are the same as those listed above in order.

Overexpression Studies in Human Cancer Cell Lines. Stable INPP1 overexpression was achieved by subcloning the INPP1 gene into the pMSCVpuro vector (Clontech), generating retrovirus using the AmphiPack-293 Cell Line, as described above with the RNA interference studies. The human INPP1 was subcloned into the pMSCVpuro (Clontech) by using XhoI and EcoRI restriction sites using the following primers 5'-GTACGTACCTCGAAGATAT-CCTCCGG-3' and 5'-GTACGTACGAATTATGCGTCTCTGC-

3'. For transient overexpression of INPP1 in SKOV3 cells, cells were seeded in 6-cm dishes (200,000 cells) for 24 h and then transfected with human INPP1 (in the mammalian SPORT6 expression vector). At 48 h post transfection, cells were harvested for either RNA extraction or metabolomics. For simultaneous transient mouse INPP1 overexpression and siINPP1 knockdown, cells were seeded in 6-cm dishes (200,000 cells) for 24 h and then transfected simultaneously with siINPP1 #1 as well as with a mouse INPP1 overexpression construct.

Cell Migration, Cell Survival, Cell Proliferation, and Invasion Studies. Migration, invasion, cell proliferation, and survival studies were performed as described previously.⁴ Migration assays were performed in Transwell chambers (Corning) with 8- μ m pore-sized membranes coated with collagen in which 50,000 cells were seeded into the top chamber and chambers with fixed with Diff-Quik solutions 5 h after seeding cells per manufacturer's instructions (Dade Behring). Cells that had not migrated through the chamber on the top of the chamber were removed with a cotton ball, and migrated cells were counted at a magnification of 400 \times . An average of cells in 4 fields for one migration chamber represents $n = 1$. Cell survival and proliferation assays were performed using the Cell Proliferation Reagent WST-1 (Roche) as previously described.⁴ Cells were washed twice in PBS, harvested by trypsinization, washed in serum-free media, and seeded into 96-well plates (10,000 cells for proliferation, and 20,000 cells for cell survival) in a volume of 200 μ L for 0 and 24 h prior to addition of WST-1 (20 μ L) for 1 h at 37 °C in 5% CO₂. Absorbance was then measured at 450 nm using a spectrophotometer. Invasion assays were conducted using the BD Matrigel Invasion Chambers per the manufacturer's protocol.

Tumor Xenograft Studies. Human cancer xenografts were established by transplanting cancer cell lines ectopically into the flank of C.B17 SCID mice (Taconic Farms) as described previously.⁴ Briefly, cells were washed two times with PBS, trypsinized, and harvested in serum-containing medium. Next, the harvested cells were washed two times with serum-free medium and resuspended at a concentration of 2.0×10^4 cells/mL and 100 μ L was injected. Growth of the tumors was measured every 3 days with calipers.

Metabolomic Profiling of Cancer Cells. Metabolite measurements were conducted using modified previous procedures.^{4,22} Cancer cells were grown in serum-free media for 4 h to minimize the contribution of serum-derived metabolites to the cellular profiles. Cancer cells (1×10^6 cells/6-cm dish or 2×10^6 cells/6-cm dish for nonpolar and polar metabolomics, respectively) were washed twice with phosphate buffer saline (PBS), harvested by scraping, and isolated by centrifugation at 1400g at 4 °C, and cell pellets were flash frozen and stored at –80 °C until metabolome extractions. Nonpolar lipid metabolites were extracted in 4 mL of a 2:1:1 mixture of chloroform/methanol/Tris buffer with inclusion of internal standards C12:0 dodecylglycerol (10 nmol) and pentadecanoic acid (10 nmol). Organic and aqueous layers were separated by centrifugation at 1000g for 5 min, and the organic layer was collected. The aqueous layer was acidified (for metabolites such as LPA) by adding 0.1% formic acid, followed by the addition of 2 mL of chloroform. The mixture was vortexed, and the organic layers were combined, dried down under N₂, and dissolved in 120 μ L of chloroform, of which 10 μ L was analyzed by both single-reaction monitoring (SRM)-based LC–MS/MS or untargeted LC–MS. LC separation was achieved with a Luna reverse-phase C5 column (50 mm × 4.6 mm with 5 μ m diameter particles, Phenomenex). Mobile phase A was composed of a 95:5 ratio of water/methanol, and mobile phase B consisted of 2-propanol/methanol/water in a 60:35:5 ratio. Solvent modifiers 0.1% formic acid with 5 mM ammonium formate and 0.1% ammonium hydroxide were used to assist ion formation as well as to improve the LC resolution in both positive and negative ionization modes, respectively. The flow rate for each run started at 0.1 mL/min for 5 min, to alleviate backpressure associated with injecting chloroform. The gradient started at 0% B and increased linearly to 100% B over the course of 45 min with a flow rate of 0.4 mL/min, followed by an isocratic gradient of 100% B for 17 min at 0.5 mL/min before equilibrating for 8 min at 0% B with a flow rate of 0.5 mL/min.

Frozen cell pellets for polar metabolomic analyses were extracted in 180 μ L of 40:40:20 acetonitrile/methanol/water with inclusion of internal standard d_3 -serine (10 nmol). Following 30 s of thorough vortexing and 1 min of bath sonication, the polar metabolite fraction (supernatant) was isolated by centrifugation at 13,000g for 15 min. Twenty microliters of this supernatant was analyzed by SRM-based targeted or untargeted LC–MS/MS. For separation of polar metabolites, normal-phase chromatography was performed with a Luna-5 mm NH₂ column (50 mm \times 4.60 mm, Phenomenex). Mobile phases were as follows: Buffer A, acetonitrile; Buffer B, 95:5 water/acetonitrile with 0.1% formic acid or 0.2% ammonium hydroxide with 50 mM ammonium acetate for positive and negative ionization mode, respectively. The flow rate for each run started at 0.2 mL/min for 5 min, followed by a gradient starting at 0% B and increasing linearly to 100% B over the course of 45 min with a flow rate of 0.7 mL/min, followed by an isocratic gradient of 100% B for 17 min at 0.7 mL/min before equilibrating for 8 min at 0% B with a flow rate of 0.7 mL/min.

MS analysis was performed with an electrospray ionization (ESI) source on an Agilent 6430 QQQ LC–MS/MS. The capillary voltage was set to 3.0 kV, and the fragmentor voltage was set to 100 V. The drying gas temperature was 350 °C, the drying gas flow rate was 10 L/min, and the nebulizer pressure was 35 psi. For both polar and nonpolar targeted metabolomic analysis, representative metabolites were quantified by SRM of the transition from precursor to product ions at associated collision energies. These values and associated retention times are listed in Supplementary Table 1. Untargeted LC–MS was performed by scanning a mass range of *m/z* 50–1200, and data were exported as mzdata files and uploaded to XCMSOnline (xcmsserver.nutr.berkeley.edu) to identify metabolites that were differentially changed. These metabolites from untargeted analysis were putatively identified through using the METLIN online database. Standards were purchased to confirm coelution and fragmentation of the standard with the metabolite of interest. This metabolite was then quantified by SRM analysis. Metabolites were quantified by integrating the area under the peak and were normalized to internal standard values, and then levels were expressed as percent of control.

We have also extracted cells directly on the cell culture dish by pipetting 180 μ L of –20 °C 40:40:20 acetonitrile/methanol/water directly onto the cells, followed by vortexing the resulting cellular metabolome mixture and centrifugation at 10,000g for 10 min. The supernatant was then analyzed by SRM-based analysis, and isotopic levels of glycolytic intermediates from [¹³C]glucose labeling of cells for 24 h were compared between the on-plate extraction procedure and extraction of isolated cell pellets kept at –80 °C. We find that there is no difference in the levels of isotopically incorporated glycolytic intermediates between the on-plate extraction compared with the extraction of isolated cell pellets (data not shown).

Analysis of Steady-State Isotopic Incorporation into Glycolytic Metabolites. Steady-state isotopic glycolytic metabolism was measured by labeling cells with [¹²C] or [¹³C]glucose and quantifying both nonisotopic and isotopic incorporation into glycolytic intermediates. Cells were treated with either 10 mM [¹²C]glucose or [¹³C]glucose in glucose-free RPMI media, 48 h following transfection of cells with siControl or siINPP1 oligonucleotides. Cells were harvested 24 h after labeling with [¹²C]/[¹³C]glucose, and the polar metabolome was extracted as previously described and analyzed by SRM-based targeted LC–MS/MS for both nonisotopic and isotopic glycolytic intermediates.

Western Blotting. Cells were lysed by probe sonication in PBS containing both protease and phosphatase inhibitors. Proteins were resolved by electrophoresis on 4–15% Tris-glycine precast Mini-PROTEAN TGX gel (BioRad Laboratories) and transferred to PVDF membranes using the iBlot system (Invitrogen). Blots were blocked with 5% nonfat milk in a Tris-buffered saline containing Tween-20 (TBST) solution for 60 min at RT, washed in 1x TBST, and probed with primary antibody of interest diluted in 5% BSA TBST solution. Following 3 subsequent TBST washes, the blots were incubated in the dark with a IR-linked secondary at RT for 1 h. Following 3 more washes, blots were visualized using an Odyssey Li-Cor scanner.

Oncogene Overexpression in MCF10A Cells. We will fully describe the generation of these lines in a subsequent manuscript. Briefly, the oncogenes described in Supplementary Figure S were stably expressed in MCF10A cells, and infected cells were selected by puromycin.

Glucose Consumption. Glucose consumption from RPMI media was measured by collecting media and performing a colorimetric glucose assay using a kit purchased from Abcam per the manufacturers protocol.

ASSOCIATED CONTENT

Supporting Information

Supplemental methods, figures, and tables. This material is available free of charge via the Internet at <http://pubs.acs.org>.

AUTHOR INFORMATION

Corresponding Author

*E-mail: dnomura@berkeley.edu.

Notes

The authors declare no competing financial interest.

ACKNOWLEDGMENTS

We thank the members of the Nomura laboratory for helpful discussion and critical reading of the manuscript. This work was supported by the National Institutes of Health (R00DA030908, R01CA172667, R21CA170317, 5R01CA170447, SR01CA136717) and the Searle Scholar Foundation (D.K.N., S.M.L., M.M.M., R.A.K., A.C., A.O., A.G.). S.-W.N. was partly supported by 1R21CA150237 and R01CA172667.

REFERENCES

- (1) Vander Heiden, M. G., Cantley, L. C., and Thompson, C. B. (2009) Understanding the Warburg effect: the metabolic requirements of cell proliferation. *Science* 324, 1029–1033.
- (2) Benjamin, D. I., Cravatt, B. F., and Nomura, D. K. (2012) Global profiling strategies for mapping dysregulated metabolic pathways in cancer. *Cell Metab.* 16, 565–577.
- (3) Nomura, D. K., Lombardi, D. P., Chang, J. W., Niessen, S., Ward, A. M., Long, J. Z., Hoover, H. H., and Cravatt, B. F. (2011) Monoacylglycerol lipase exerts dual control over endocannabinoid and fatty acid pathways to support prostate cancer. *Chem. Biol.* 18, 846–856.
- (4) Nomura, D. K., Long, J. Z., Niessen, S., Hoover, H. S., Ng, S. W., and Cravatt, B. F. (2010) Monoacylglycerol lipase regulates a fatty acid network that promotes cancer pathogenesis. *Cell* 140, 49–61.
- (5) Chiang, K. P., Niessen, S., Saghatelian, A., and Cravatt, B. F. (2006) An enzyme that regulates ether lipid signaling pathways in cancer annotated by multidimensional profiling. *Chem. Biol.* 13, 1041–1050.
- (6) Chang, J. W., Nomura, D. K., and Cravatt, B. F. (2011) A potent and selective inhibitor of KIAA1363/AADACL1 that impairs prostate cancer pathogenesis. *Chem. Biol.* 18, 476–484.
- (7) Inhorn, R. C., and Majerus, P. W. (1987) Inositol polyphosphate 1-phosphatase from calf brain. Purification and inhibition by Li⁺, Ca²⁺, and Mn²⁺. *J. Biol. Chem.* 262, 15946–15952.
- (8) Li, S. R., Gyselman, V. G., Lalude, O., Dorudi, S., and Bustin, S. A. (2000) Transcription of the inositol polyphosphate 1-phosphatase gene (INPP1) is upregulated in human colorectal cancer. *Mol. Carcinog.* 27, 322–329.
- (9) Sethi, N., and Kang, Y. (2011) Unravelling the complexity of metastasis - molecular understanding and targeted therapies. *Nat. Rev. Cancer* 11, 735–748.
- (10) Nguyen, D. X., Bos, P. D., and Massague, J. (2009) Metastasis: from dissemination to organ-specific colonization. *Nat. Rev. Cancer* 9, 274–284.

- (11) Sebolt-Leopold, J. S., and Herrera, R. (2004) Targeting the mitogen-activated protein kinase cascade to treat cancer. *Nat. Rev. Cancer* **4**, 937–947.
- (12) Tautenhahn, R., Patti, G. J., Rinehart, D., and Siuzdak, G. (2012) XCMS Online: a web-based platform to process untargeted metabolomic data. *Anal. Chem.* **84**, 5035–5039.
- (13) Mills, G. B., and Moolenaar, W. H. (2003) The emerging role of lysophosphatidic acid in cancer. *Nat. Rev. Cancer* **3**, 582–591.
- (14) Ohta, H., Sato, K., Murata, N., Damirin, A., Malchinkhuu, E., Kon, J., Kimura, T., Tobo, M., Yamazaki, Y., Watanabe, T., Yagi, M., Sato, M., Suzuki, R., Murooka, H., Sakai, T., Nishitoba, T., Im, D. S., Nochi, H., Tamoto, K., Tomura, H., and Okajima, F. (2003) Ki16425, a subtype-selective antagonist for EDG-family lysophosphatidic acid receptors. *Mol. Pharmacol.* **64**, 994–1005.
- (15) Elstrom, R. L., Bauer, D. E., Buzzai, M., Karnauskas, R., Harris, M. H., Plas, D. R., Zhuang, H., Cinalli, R. M., Alavi, A., Rudin, C. M., and Thompson, C. B. (2004) Akt stimulates aerobic glycolysis in cancer cells. *Cancer Res.* **64**, 3892–3899.
- (16) Zhong, D. S., Xiong, L., Liu, T. R., Liu, X. J., Liu, X. G., Chen, J., Sun, S. Y., Khuri, F. R., Zong, Y. P., Zhou, Q. H., and Zhou, W. (2009) The glycolytic inhibitor 2-deoxyglucose activates multiple prosurvival pathways through IGF1R. *J. Biol. Chem.* **284**, 23225–23233.
- (17) Yu, F. X., Zhao, B., Panupinthu, N., Jewell, J. L., Lian, I., Wang, L. H., Zhao, J., Yuan, H., Tumaneng, K., Li, H., Fu, X. D., Mills, G. B., and Guan, K. L. (2012) Regulation of the Hippo-YAP pathway by G-protein-coupled receptor signaling. *Cell* **150**, 780–791.
- (18) Cai, H., and Xu, Y. (2013) The role of LPA and YAP signaling in long-term migration of human ovarian cancer cells. *Cell Commun. Signaling* **11**, 31.
- (19) Yang, W., Xia, Y., Cao, Y., Zheng, Y., Bu, W., Zhang, L., You, M. J., Koh, M. Y., Cote, G., Aldape, K., Li, Y., Verma, I. M., Chiao, P. J., and Lu, Z. (2012) EGFR-induced and PKC ϵ monoubiquitylation-dependent NF-kappaB activation upregulates PKM2 expression and promotes tumorigenesis. *Mol. Cell* **48**, 771–784.
- (20) Babic, I., Anderson, E. S., Tanaka, K., Guo, D., Masui, K., Li, B., Zhu, S., Gu, Y., Villa, G. R., Akhavan, D., Nathanson, D., Gini, B., Mareninov, S., Li, R., Camacho, C. E., Kurdistani, S. K., Eskin, A., Nelson, S. F., Yong, W. H., Cavenee, W. K., Cloughesy, T. F., Christofk, H. R., Black, D. L., and Mischel, P. S. (2013) EGFR mutation-induced alternative splicing of Max contributes to growth of glycolytic tumors in brain cancer. *Cell Metab.* **17**, 1000–1008.
- (21) Jessani, N., Humphrey, M., McDonald, W. H., Niessen, S., Masuda, K., Gangadharan, B., Yates, J. R., Mueller, B. M., and Cravatt, B. F. (2004) Carcinoma and stromal enzyme activity profiles associated with breast tumor growth in vivo. *Proc. Natl. Acad. Sci. U.S.A.* **101**, 13756–13761.
- (22) Kopp, F., Komatsu, T., Nomura, D. K., Trauger, S. A., Thomas, J. R., Siuzdak, G., Simon, G. M., and Cravatt, B. F. (2010) The glycerophospho metabolome and its influence on amino acid homeostasis revealed by brain metabolomics of GDE1(−/−) mice. *Chem. Biol.* **17**, 831–840.